Diabatically Induced Secondary Flows in Tropical Cyclones. Part II: Periodic Forcing

HUGH E. WILLOUGHBY

Department of Earth Sciences, Florida International University, Miami, Florida

(Manuscript received 20 May 2008, in final form 15 August 2008)

ABSTRACT

The linearized equation for the time-varying, axially symmetric circumferential component of the vorticity in a hurricane-like vortex closely resembles the classical Sawyer–Eliassen equation for the quasi-steady, diabatically induced secondary-flow streamfunction. The salient difference lies in the coefficients of the second partial derivatives with respect to radius and height. In the Sawyer–Eliassen equation, they are the squares of the buoyancy and isobaric local inertia frequencies; in the circumferential vorticity equation they are the differences between these quantities and the square of the frequency with which the imposed forcing varies. The coefficient of the mixed partial derivative with respect to radius and height is the same in both equations. Thus, for low frequencies the response to periodic forcing is a slowly varying analog to steady Sawyer–Eliassen solutions. For high frequencies, the solutions are radially propagating inertia-buoyancy waves. Since the local inertia frequency, which approximately defines the boundary between quasi-steady and propagating solutions, decreases with radius, quasi-steady solutions in the vortex core transform into radiating ones far from the center. Periodic forcing will always lead to some wave radiation to the storm environment unless the period of the forcing is longer than a half-pendulum day.

1. Introduction

Tropical cyclones (TCs) intensify by convective release of latent heat drawn from the sea (e.g., Emanuel 1999). This heating, which is concentrated in the eyewall, forces a quasi-steady secondary flow composed of low-level mass convergence, eyewall updrafts, and upper-tropospheric divergence (Pendergrass and Willoughby 2009, hereafter Part I, and references therein). The low-level convergence imports angular momentum, causing the axially symmetric primary vortex to intensify while maintaining gradient balance between the momentum and mass distributions. To keep the primary vortex nearly balanced, the forcing must change slowly, be weak enough to keep the induced secondary flow small relative to the primary flow, and be predominantly symmetric about the axis of vortex rotation (e.g., Shapiro and Willoughby 1982).

In quantitative terms, balance requires that the characteristic time for appreciable intensity change be long compared with the local inertial period $2\pi/I$ in a neighborhood around the locus of heating. The square of the local inertia frequency, I^2, is defined to be the radial gradient of the square of the angular momentum divided by the cube of the radius. The local inertia period at the radius of maximum wind (RMW) can vary from a half hour to several hours, dependent upon TC size and strength. It decreases asymptotically to a half-pendulum day far from the center. When the steadiness, forcing weakness, and symmetry conditions are met, the Sawyer–Eliassen equation (SEQ) can be used to compute the secondary flow as a heating-induced, quasi-steady mass flow streamfunction (e.g., Part I). Advection of primary flow angular momentum and mass by the secondary flow is the agent of intensification. In the ''convective ring'' model, the secondary flow penetrates from the eyewall a short distance across a strong radial gradient of angular momentum into the eye, increasing the wind at the radius of maximum wind and inward from it, so that the eye contracts as the maximum wind strengthens (Smith 1981; Schubert and Hack 1982; Shapiro and Willoughby 1982; Willoughby et al. 1982).

Derivation of the SEQ replaces the vertical and radial momentum equations by gradient wind and hydrostatic balance, deduces the swirling wind tendency both from the tangential momentum equation and from the thermodynamic energy equation recast as a thermal wind

Corresponding author address: H. E. Willoughby, Department of Earth Sciences, Florida International University, University Park Campus, PC 344, Miami, FL 33199.
E-mail: hugh.willoughby@fiu.edu

DOI: 10.1175/2008MWR2658.1

tendency equation, and eliminates the time derivative to produce a diagnostic equation for the secondary flow. The result is actually a diagnostic equation for the circumferential component of the vorticity that balances production by solenoidal heating with dissipation by work done against buoyancy forces distant from the heat source. Thus, the SEQ does not require explicit friction to limit the growth of the circumferential vorticity. Essential to validity of the SEQ are the previously enumerated conditions of gradual change, primary flow much stronger than secondary flow, and axial symmetry.

Time-varying (specifically, periodic) forcing requires a different formulation in which the governing equations are linearized about the primary vortex. As shown in the next section, algebraic elimination of all variables except the radial and vertical velocities leaves an equation for the circumferential component of the vorticity (e.g., Pearce 2004, 2005; Smith 2005) in which the perturbation vortex tubes encircle the vortex. Like the SEQ, this equation is a second-order partial differential equation for the mass flow streamfunction, but one that relaxes the requirements for gradient and hydrostatic balance. In the SEQ, the coefficients of the second partial derivatives with respect to radius and height are the squares of the buoyancy and inertia frequencies. In the circumferential vorticity equation (CVE), these coefficients are the differences between the squares of the buoyancy and inertia frequencies and the square of the frequency of periodic forcing. In both equations, the coefficient of the mixed partial derivative is proportional to the mean radial buoyancy gradient. For frequencies within the passband defined by its discriminant, the CVE is hyperbolic and its solutions are radiating inertia-buoyancy waves. For frequencies below the passband, the CVE is elliptic with quasi-steady secondary circulation solutions like those described by the SEQ. Since the inertia frequency decreases with distance from the center, the solution's character changes radially. When the forcing oscillates slowly in time, the solution in the core is quasi steady, but beyond 50–200 km from the center it transforms into low-frequency radiating waves. Here we retain the traditional name for the SEQ, and apply "CVE" to the explicitly time-dependant equation, even though both describe the circumferential vorticity.

The conventional view is that tropical cyclones, in common with many geophysical fluid systems, may be modeled as a slowly varying basic flow with more rapidly changing perturbations superimposed. This paradigm was the rationale for the pioneering hurricane models (e.g., Ooyama 1969; Sundquist 1970). A key question in this context is the meaning of "slowly varying." Scale analysis suggests that the mean flow should not change significantly over a few orbital periods for air circling the storm with the mean swirling wind (Shapiro and Willoughby 1982). It is clear observationally (e.g., Malkus et al. 1961) that underlying hurricane vortex and even many of the asymmetric features evolve on synoptic time scales, despite their mesoscale spatial scales. According to the "hot tower" hypothesis (Simpson et al. 1998; Hendricks et al. 2004; Montgomery et al. 2006), which runs contrary to the balance paradigm, episodically released convective energy, after cascading upward to an axially symmetric spatial scale and a long (many orbital periods) time scale, can power evolution of the mean vortex. What the present analysis offers is a means to analyze tropical cyclone responses to axially symmetric, periodic heating on time scales that vary from the buoyancy period to about a pendulum day.

2. Analysis

As in Part I, the axially symmetric mean vortex in gradient and hydrostatic balance is described by

$$\frac{v_0^2}{r} + fv_0 = c_p\theta_0\frac{\partial \pi_0}{\partial r}, \tag{1a}$$

$$\frac{\partial \pi_0}{\partial z} = -\frac{g}{c_p\theta_0}. \tag{1b}$$

Here, $v_0(r,z)$ is the mean vortex swirling flow; $\pi_0(r,z) = (p_0/1000)^{R/c_p}$ is the mean Exner function computed from pressure, $p_0(r, z)$ and the gas constant and specific heat at constant pressure for dry air, R and c_p; and $\theta_0(r,z) = T_0(1000/p_0)^{R/c_p}$ is the potential temperature corresponding to the mean virtual temperature $T_0(r,z)$. The mass field is in thermal wind balance with the mean vortex wind. These equations are set in height coordinates; r is radius and z is geometric height, g is the gravitational acceleration, and f is the Coriolis parameter. We define a mean state buoyancy $b_0(r,z) = g\ln(\theta_0/273.16)$. The linear governing equations for axially symmetric perturbations oscillating with frequency ω on this vortex are

$$-i\omega v + \zeta u + Sw = M, \tag{2a}$$

$$-i\omega u - \xi v + \gamma b = -c_p\theta_0\frac{\partial \pi}{\partial r}, \tag{2b}$$

$$-i\omega w - b = -c_p\theta_0\frac{\partial \pi}{\partial z}, \tag{2c}$$

$$-i\omega b + Bu + N^2 w = Q', \quad \text{and} \tag{2d}$$

$$\frac{\partial(r\rho u)}{\partial r} + \frac{\partial(r\rho w)}{\partial z} = 0. \tag{2e}$$

The perturbation velocities in the radial, tangential, and vertical directions are $u(r, z, t)$, $v(r, z, t)$, and $w(r, z, t)$; the perturbation Exner function is $\pi(r, z, t)$; and

$b(r,z,t) = g[\theta(r,z,t) - \theta_0(r,z)]/\theta_0(r,z)$is the perturbation buoyancy corresponding to perturbation virtual potential temperature $\theta(r,z,t)$. All perturbation quantities are complex such that their real parts are in phase with the forcing, which is strictly real, and the imaginary parts lag it by $\pi/2$. The vortex has mean flow vertical vorticity, $\zeta = \partial v_0/\partial r + v_0/r + f$, inertia parameter, $\xi = 2v_0/r + f$, and shear $S = \partial v_0/\partial z$. The radial and vertical gradients of the mean vortex buoyancy are $B = \partial b_0/\partial r$ and $N^2 = \partial b_0/\partial z$. Here B, which has units of s^{-2} is the baroclinic term and N^2 is the square of the buoyancy, or Brunt-Väisälä frequency: $\partial N^2/\partial r = \partial B/\partial z$. The mean-state air density is $\rho = 1000\pi_0^{c_v/R}/R\theta_0$, where c_v is the specific heat of dry air at constant volume. Here $Q' = (gq/c_p\theta_0)$is the diabatic perturbation buoyancy source where q is the actual heating rate. The mean flow thermal wind relation, obtained by vertical differentiation of (1a) is $B = \xi S - \gamma N^2$, where $\gamma = g^{-1}(v^2/r + fv)$ is ratio of the mean-flow radial acceleration to gravity, or equivalently the slope of isobaric surfaces in pressure coordinates.

Introduction of a mass flow streamfunction $\psi(r,z)$, such that

$$r\rho u = -\frac{\partial \psi}{\partial z}, \quad r\rho w = \frac{\partial \psi}{\partial r}, \tag{3}$$

insures mass continuity for the secondary flow. Differentiation with respect to time and algebraic elimination of the tangential wind and buoyancy between (2b) and (2c) yields

$$(I^2 - \gamma B^2 - \omega^2)u + Bw - \xi M + \gamma Q = c_p\theta_0 i\omega\frac{\partial \pi}{\partial r}, \tag{4a}$$

$$Bu + (N^2 - \omega^2)w - Q = c_p\theta_0 i\omega\frac{\partial \pi}{\partial z}, \tag{4b}$$

where $I^2 = \zeta\xi$ is the local inertia frequency. The quantity $I^2 - \gamma B^2 = I'^2$ is the isobaric inertia frequency that takes into account projection of isobaric static stability onto horizontal surfaces that arises from the difference in slope between constant p and constant z surfaces. Cross differentiation of (4a) and (4b) produces

$$\frac{\partial}{\partial z}[(I'^2 - \omega^2)u + Bw] - \frac{\partial}{\partial z}(\xi M - \gamma Q) = \frac{1}{\theta_o}\frac{\partial \theta_0}{\partial z}c_p\theta_0 i\omega\frac{\partial \pi}{\partial r} + c_p\theta_0 i\omega\frac{\partial^2 \pi}{\partial r\partial z}, \tag{5a}$$

$$\frac{\partial}{\partial r}[Bu + (N^2 - \omega^2)w] - \frac{\partial}{\partial r}Q = \frac{1}{\theta_o}\frac{\partial \theta_0}{\partial r}c_p\theta_0 i\omega\frac{\partial \pi}{\partial z} + c_p\theta_0 i\omega\frac{\partial^2 \pi}{\partial r\partial z}. \tag{5b}$$

Substituting from (4a) and (4b) and rearranging yields

$$\left(\frac{\partial}{\partial z} - \frac{1}{\theta_0}\frac{\partial \theta_0}{\partial z}\right)[(I'^2 - \omega^2)u + Bw] - \left(\frac{\partial}{\partial z} - \frac{1}{\theta_0}\frac{\partial \theta_0}{\partial z}\right)(\xi M - \gamma Q) = c_p\theta_0 i\omega\frac{\partial^2 \pi}{\partial r\partial z}, \tag{6a}$$

$$\left(\frac{\partial}{\partial r} - \frac{1}{\theta_0}\frac{\partial \theta_0}{\partial r}\right)[Bu + (N^2 - \omega^2)w] - \left(\frac{\partial}{\partial r} - \frac{1}{\theta_0}\frac{\partial \theta_0}{\partial r}\right)Q = c_p\theta_0 i\omega\frac{\partial^2 \pi}{\partial r\partial z}. \tag{6b}$$

Elimination of the right-hand sides by subtraction and substitution from (3) leaves a single equation for the streamfunction response to diabatic and momentum forcing:

$$\left(\frac{\partial}{\partial r} - \frac{1}{\theta_0}\frac{\partial \theta_0}{\partial r}\right)\left[(N^2 - \omega^2)\frac{1}{r\rho}\frac{\partial \psi}{\partial r} - B^2\frac{1}{r\rho}\frac{\partial \psi}{\partial z}\right] + \left(\frac{\partial}{\partial z} - \frac{1}{\theta_0}\frac{\partial \theta_0}{\partial z}\right)\left[(I'^2 - \omega^2)\frac{1}{r\rho}\frac{\partial \psi}{\partial z} - B^2\frac{1}{r\rho}\frac{\partial \psi}{\partial r}\right] = \left(\frac{\partial}{\partial r} - \frac{1}{\theta_0}\frac{\partial \theta_0}{\partial r}\right)Q - \left(\frac{\partial}{\partial z} - \frac{1}{\theta_0}\frac{\partial \theta_0}{\partial z}\right)(\xi M - \gamma Q). \tag{7}$$

Expanding the derivatives of density and radius inside the brackets, defining

$$\frac{1}{R_{\theta\rho}} \equiv \frac{1}{r} + \frac{1}{\theta_0}\frac{\partial \theta_0}{\partial r} + \frac{1}{\rho}\frac{\partial \rho}{\partial r},$$

$$\frac{1}{H_{\theta\rho}} \equiv \frac{1}{\theta_0}\frac{\partial \theta_0}{\partial z} + \frac{1}{\rho}\frac{\partial \rho}{\partial z},$$

$$\frac{1}{L_\theta} \equiv \frac{1}{\theta_0}\frac{\partial \theta_0}{\partial r}, \quad \text{and}$$

$$\frac{1}{H_\theta} \equiv \frac{1}{\theta_0}\frac{\partial \theta_0}{\partial z},$$

substituting, and expanding the derivatives simplifies (7) to

$$(N^2 - \omega^2)\frac{\partial^2 \psi}{\partial r^2} - 2B\frac{\partial^2 \psi}{\partial r\partial z} + (I'^2 - \omega^2)\frac{\partial^2 \psi}{\partial z^2} - \left[\frac{(N^2 - \omega^2)}{R_{\theta\rho}} - \frac{B}{H_{\theta\rho}}\right]\frac{\partial \psi}{\partial r} - \left[\frac{(I'^2 - \omega^2)}{H_{\theta\rho}} - \frac{B}{R_{\theta\rho}}\right]\frac{\partial \psi}{\partial z} + \left(\frac{\partial N^2}{\partial r} - \frac{\partial B}{\partial z}\right)\frac{\partial \psi}{\partial r} + \left(\frac{\partial I'^2}{\partial z} - \frac{\partial B}{\partial r}\right)\frac{\partial \psi}{\partial z} = r\rho\left[\left(\frac{\partial}{\partial r} - \frac{1}{L_\theta}\right)Q - \left(\frac{\partial}{\partial z} - \frac{1}{H_\theta}\right)(\xi M - \gamma Q)\right]. \tag{8}$$

The identities $\partial B/\partial r = \partial I'^2/\partial z - 3\xi S/r + B\partial\gamma/\partial z - N^2\partial\gamma/\partial r$, and $\partial B^2/\partial r = \partial N^2/\partial z$ transform (8) to

$$(N^2-\omega^2)\frac{\partial^2\psi}{\partial r^2}-2B\frac{\partial^2\psi}{\partial r\partial z}+(I'^2-\omega^2)\frac{\partial^2\psi}{\partial z^2}$$
$$-\left[\frac{(N^2-\omega^2)}{R_{\theta\rho}}-\frac{B}{H_{\theta\rho}}\right]\frac{\partial\psi}{\partial r}$$
$$-\left[\frac{(I'^2-\omega^2)}{H_{\theta\rho}}-\frac{B}{R_{\theta\rho}}-\frac{3\xi S}{r}+B\frac{\partial\gamma}{\partial z}-N^2\frac{\partial\gamma}{\partial r}\right]\frac{\partial\psi}{\partial z}$$
$$=r\rho\left[\left(\frac{\partial}{\partial r}-\frac{1}{L_\theta}\right)Q-\left(\frac{\partial}{\partial z}-\frac{1}{H_\theta}\right)(\xi M-\gamma Q)\right]. \quad (9)$$

Equation (9) resembles the diagnostic SEQ [see (9) in Part I], but describes periodic perturbations on a balanced vortex induced by periodically varying heating rather than the gradual evolution of the balanced vortex itself in response to steady heating. In (9), N^2 and I'^2 from Part I are everywhere replaced by $N^2-\omega^2$ and $I'^2-\omega^2$, respectively. In contrast with the SEQ, the perturbations are not necessarily in either hydrostatic or gradient balance, although the mean vortex is. This equation is readily solved numerically on an r–z grid using the direct solution method of Lindzen and Kuo (1969). One of the virtues of this algorithm is its robustness to changes in the character of the PDE from elliptic to hyperbolic.

The domain used here extends vertically to 30 km, 50% deeper than that used in Part I. Its radial extent is 1500 km, although only the inner 200–400 km are illustrated here. Vertical and horizontal grid resolutions are 1.5 and 2 km. At the surface and center boundaries $\psi=0$ insuring no axially symmetric flow into the sea surface or across the center. At the outer boundary $\partial\psi/\partial r=0$, so that flow into or out of the domain there is strictly horizontal. At the top we impose a radiation boundary condition, combined with a sponge layer of strong Newtonian dissipation above 23.5 km. The dissipation rate is 1/600 s. The damping increases linearly to the maximum from 16 km to the top of the domain. At the outer boundary the damping increases linearly to the same maximum from 100 km inside the boundary to the boundary itself. This treatment prevents upward-propagating waves in the stratosphere from reflecting off the domain top and back into the troposphere. Once (9) has been solved for ψ, (4) allows calculation of the velocity components. Then substitution into (2b) and inward integration of (2d) yields the buoyancy and Exner function as functions of the mean vortex structure, heating distribution, and frequency.

Clearly, when the frequency is low enough (i.e., $<<I'$), the solutions during the heating phase of the cycle should approach the quasi-steady SEQ result; whereas for frequencies (approximately) between I' and N, the solutions should project onto gravity waves. On the low-frequency side, (9) is elliptic and the heating forces a slowly varying secondary circulation with gradual evolution of the balanced mean vortex as described in Part I. However, the discriminant, $D^4=(N^2-\omega^2)(I'^2-\omega^2)-B^2$, defines a passband of frequencies,

$$\frac{1}{2}[N^2+I'^2-\sqrt{(N^2-I'^2)^2+B^4}]\le\omega^2$$
$$\le\frac{1}{2}[N^2+I'^2+\sqrt{(N^2-I'^2)^2+B^4}], \quad (10)$$

in which (9) is hyperbolic when $D^4<0$, and the solutions manifest themselves as inertia-buoyancy waves. Since I'^2 and B are strong functions of radius, (9) is often elliptic, $D^4>0$, in and near the eyewall where the forcing is applied, but becomes hyperbolic father from the center. Thus, the perturbations are balanced near the center, but become wavelike farther outward. For weakly baroclinic vortices (i.e., $N^2>>B$) power series expansion of the square roots simplifies (10) to

$$I'^2-\frac{1}{2}\frac{B^2}{N^2-I'^2}\le\omega^2\le N^2+\frac{1}{2}\frac{B^2}{N^2-I'^2}. \quad (11)$$

Thus, the baroclinic term acts to widen the passband to include frequencies below the inertia frequency and above the buoyancy frequency.

The mean vortex used here (Fig. 1a) is the ''idealized vortex'' from Part I. It has a sectionally continuous structure based upon aircraft observations in which v_0 increases linearly with radius inside the RMW and decays exponentially outside the RMW with e-folding distance 300 km. In a 20-km-wide transition zone that straddles the RMW, v_0 is a spatially varying weighted sum of the inner and outer profiles (Willoughby et al. 2006). The maximum wind is 50 m s^{-1} at the surface and shears linearly in the vertical to zero at 18.5 km. The RMW leans outward from $r=30$ km at the surface to $r=46$ km at the vortex top. The center of the imposed eyewall heating (shaded in Fig. 1a) is 2 km inside the RMW. Its axis parallels the RMW from the surface to the vortex top. As in Part I, its maximum magnitude is scaled to produce 1 m s^{-1} vertical velocity for steady forcing. Although the heating is formally complex, only the real part is nonzero so that the real part of the forced solution is in phase with the cyclic heating and the imaginary part lags it by $\pi/2$.

When the forcing is steady, the SEQ solution for this vortex and forcing has deep inflow extending to 6-km altitude outside the RMW and deep outflow reaching from ~9 km to the tropopause at 16 km (Fig. 1b). A streamfunction dipole straddles the heat source, sustaining a strong updraft coincident with the heating. Inside the RMW, the cyclonic gyre of the dipole causes gradual descent. Outside the RMW a layer of sinking

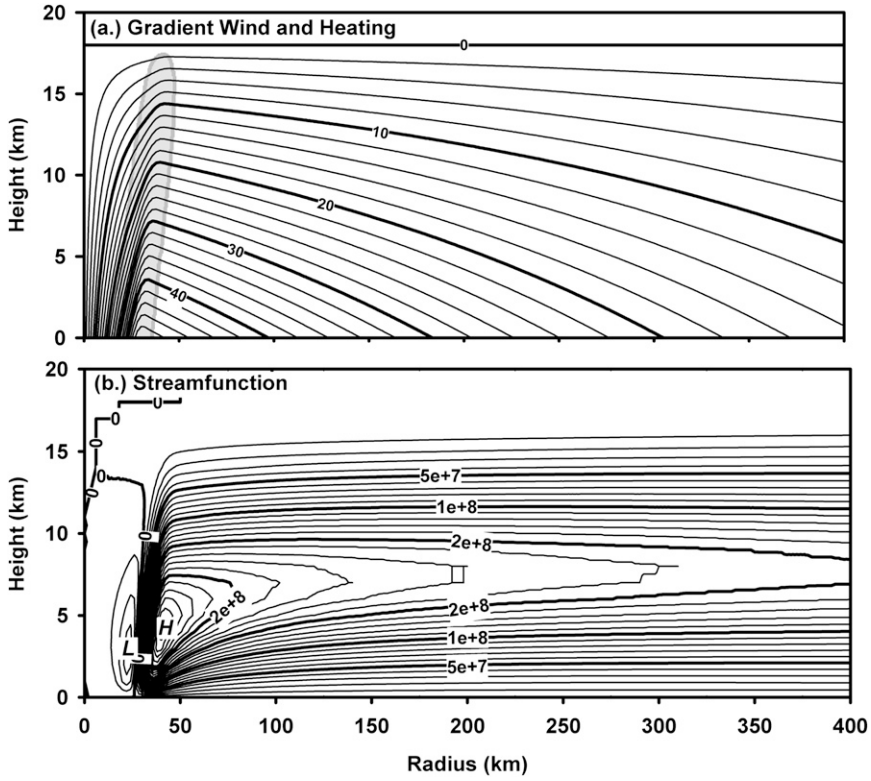

FIG. 1. (a) Mean vortex swirling wind (m s^{-1}) as a function of radius and height. Shading indicates the locus of imposed eyewall heating. (b) Mass flow streamfunction (kg s^{-1}) calculated with the SEQ for the vortex and forcing in (a).

motion extends from 3 to 5 km upward to ~8 km, separating the inflow and outflow layers. The SEQ is elliptic throughout this domain so that Fig. 1b has much in common with solutions to (9) when ω^2 is below the lower cutoff frequency defined in (11).

3. Buoyancy

Here we undertake a heuristic analysis to assess the role of buoyancy in the evolution of tangential vorticity. For simplicity we omit the vertical and radial Exner function gradients, horizontal projection of the heating, and momentum forcing from (4a) and (4b). The dynamic π-gradient terms enforce mass continuity and act as "form drag" on the buoyant updrafts (e.g., Eastin et al. 2005a,b) for high-frequency forcing and reflect hydrostatic pressure changes for low-frequency forcing. While not quantitatively rigorous, the resulting simplified equations provide a starting point for understanding buoyant response to imposed heating:

$$(I'^2 - \omega^2)u + Bw = 0, \tag{12a}$$

$$Bu + (N^2 - \omega^2)w = Q. \tag{12b}$$

The solution for u and w produces

$$u = -BQ/[(N^2 - \omega^2)(I'^2 - \omega^2) - B^2], \tag{13a}$$

$$w = (I'^2 - \omega^2)Q/[(N^2 - \omega^2)(I'^2 - \omega^2) - B^2]. \tag{13b}$$

Note that the denominator is the discriminant of (9). The slope of streamlines passing through the buoyancy source is

$$\Gamma \equiv \frac{u}{w} = \frac{-B}{(I'^2 - \omega^2)}. \tag{14}$$

Thus, when $\omega^2 < I'^2$, updrafts slope outward since $B < 0$. For very low-frequency forcing, $\Gamma \approx -S/\zeta$, so that the streamlines parallel surfaces of constant angular momentum, Λ. At higher frequencies approaching I', they are more nearly horizontal than the Λ surfaces, eventually becoming actually horizontal near $\omega^2 = I'^2$ (Fig. 2). In this neighborhood, both u and w become large. The actual singularity is not at $\omega^2 = I'^2$, but at a somewhat lower frequency consistent with (11). Throughout the frequency range $\omega^2 < I'^2$, outflow across the Λ surfaces correlates with updrafts, and the effect of heating is to decelerate the mean vortex locally. When

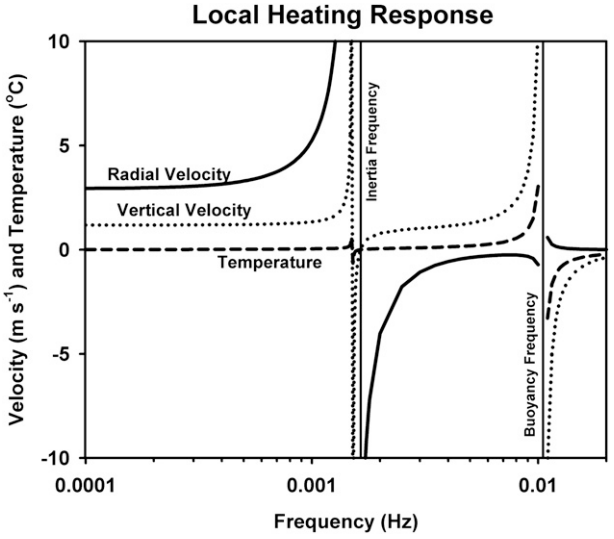

FIG. 2. Radial velocity, vertical velocity, and temperature perturbation derived from the buoyancy computed with (15a)–(15c) as functions of frequency for heat source $Q = N^2 \times 1$ m s^{-1} and values of N^2, I^2, and B representative of the eyewall.

$\omega^2 > I'^2$, updrafts correlate with inflow across Λ surfaces so that heating accelerates the mean vortex. As shown with steady heating in Part I, streamlines passing through the heat source are constrained by the π field (neglected here) to induce mass-conserving flow outside the forced subdomain. For steady eyewall heat sources, the SEQ describes induced flows that penetrate across the strong gradient of angular momentum inward from the RMW, causing $V_{\max}$ to increase and $R_{\max}$ to contract. This apparent contradiction between (14) and the full CVE solution illustrates the limitations of the simplifications introduced here.

Substitution from (14) into (13a), (13b), and (2c) yields simplified expressions for the radial and vertical flow:

$$u = \frac{\Gamma Q}{(N^2 - \omega^2) + \Gamma B}, \tag{15a}$$

$$w = \frac{Q}{(N^2 - \omega^2) + \Gamma B}, \quad \text{and} \tag{15b}$$

$$b = -i\omega w = \frac{-i\omega Q}{(N^2 - \omega^2) + \Gamma B}. \tag{15c}$$

Thus, for low frequencies ($\omega^2 \ll I'^2$)where the streamlines lean outward a little more than the Λ surfaces, the vertical velocity reflects a balance between heating and ascent in the stable stratification, The buoyancy is small, equivalent to tenths of a degree, and u and w are in phase with Q. It lags u, w, and Q by $\pi/2$. As the frequency increases, but remains $< I'$, the streamlines lean outward more steeply and the balance between heating and stable ascent is maintained. Although the buoyancy increases, it is still small until ω approaches the neighborhood of N. Somewhat paradoxically, the forcing and vertical velocity remain in phase so long as $\omega^2 < N^2$. The buoyancy lags behind both Q and w at high frequencies because inertia slows the vertical velocity, leaving some excess heating uncompensated by vertical motion. At frequencies appreciably above N all components of the response decrease rapidly with increasing ω. Despite its limitations, this analysis shows that circumferential vorticity derives from heating that causes vertical motion, but little actual buoyancy.

As shown in the next section, the apparent singularities near $|\omega| = I$ or N do not carry over into solutions of the full CVE because they are local, generally confined to a single node of the computational mesh. The dynamic π gradients neglected here force the flow to be horizontal where $|\omega| = I$ and vertical when $|\omega| = N$. Representation of (u, w) with a streamfunction enforces mass continuity. At either apparent singularity, the perpendicular velocity component is locally zero so that the streamwise derivative of the flow must also be locally zero. Thus, the streamfunction varies smoothly with well-behaved derivatives, despite the apparent singularity of the momentum equations from which it is derived. This analysis predicts an in-phase relation between the velocity components and the forcing and the phase lag between the forcing and the buoyancy. Except for frequencies near N, the buoyancy is small, as Eastin et al. (2005a,b) report and as in the complete CVE solutions obtained in the next section. The key result here is that sinusoidal diabatic forcing induces substantial vertical motions without causing the significant buoyancy perturbations hypothesized by Smith et al. (2005) unless the frequency is close to N.

4. Solutions

The discriminant is negative throughout the domain for forcing with a 60-min period (Fig. 3a). It is smaller in magnitude (i.e., less negative) near the vortex center, and increases in magnitude in the stratosphere as a result of the larger stability above the tropopause multiplied by $\sim f^2 - \omega^2$ with $\omega > f$. As anticipated above, longer forcing periods produce mixed values with $D^4 > 0$ near the center and $D^4 < 0$ farther outward. When the forcing period is 240 min (Fig. 3b), the boundary between elliptic and hyperbolic solutions starts at the surface at $r = 105$ km. It slopes upward toward the center, intersecting the eyewall near $z = 15$ km and runs horizontally across the top of the eye at that level. For still longer periods the boundary moves outward. When the period is 960 min (Fig. 3c) it leaves the surface at $r = 265$ km, slopes

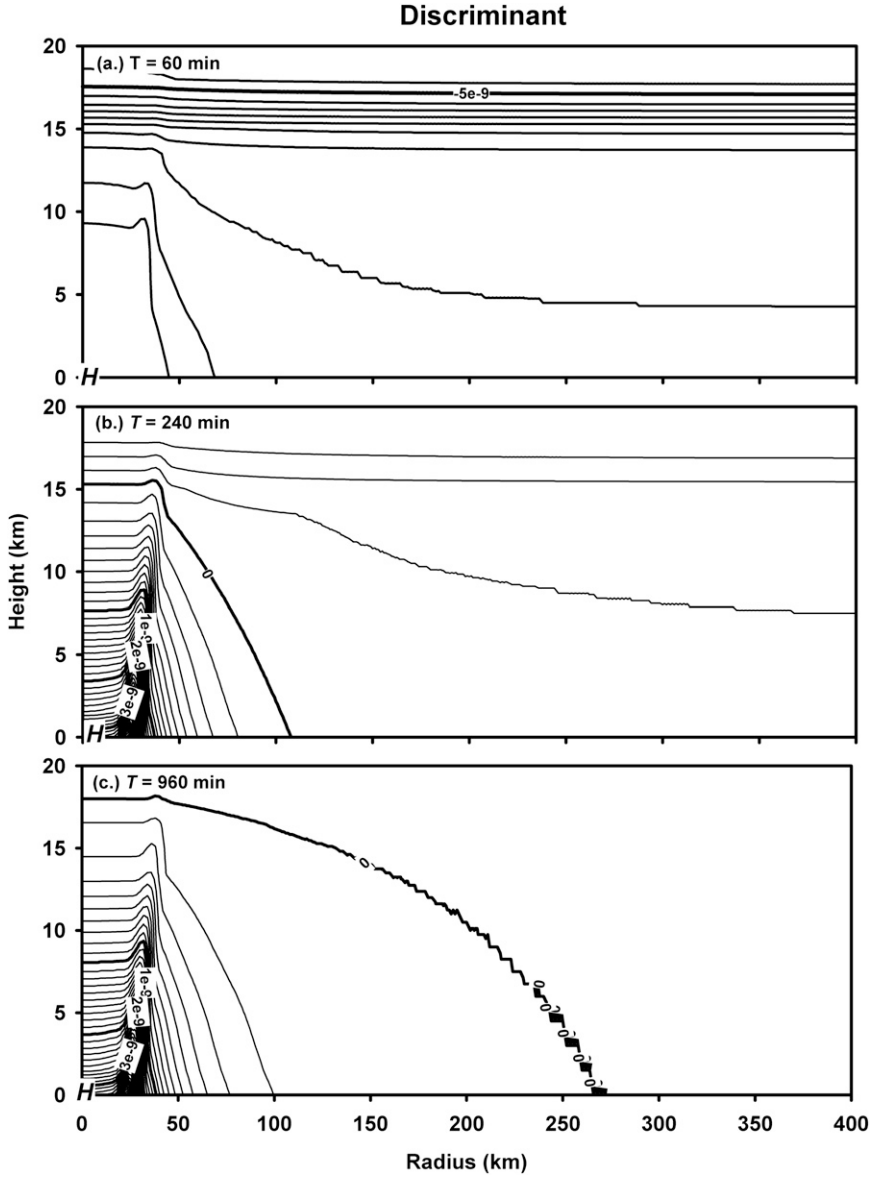

FIG. 3. The discriminant of (9) for diabatic forcing of the vortex shown in Fig. 2 with periods of (a) 60, (b) 240, and (c) 960 min.

upward, and passes over the eye in the lower stratosphere. For these low frequencies, the distribution of D^4 is dominated by N^2I^2 in the eye and within 100 km of the eyewall.

The complex streamfunctions forced by eyewall heating at 20° latitude, where a half pendulum day is 35 h, are consistent with the foregoing analysis. For periods of 30 and 60 min (Figs. 4a,b), wave energy propagates diagonally upward into the stratosphere outward from the eyewall forcing. The phase lines, which nearly parallel the group velocity, slope upward away from the forcing and refract to become somewhat more horizontal in the more stable (larger N^2) stratosphere. They propagate radially outward as they sustain an upward and outward energy flux.

With a 30-min period, the horizontal wavelength is very short. Apart from the propagation into the stratosphere around the eye, the energy scatters from the stability increase at the tropopause. It propagates outward as a wave train trapped in a tropospheric waveguide between the reflection at the surface and refraction by the faster propagation speeds of the stratosphere. As in the SEQ solution, a real streamfunction dipole straddles the heat source even when the solution is made up

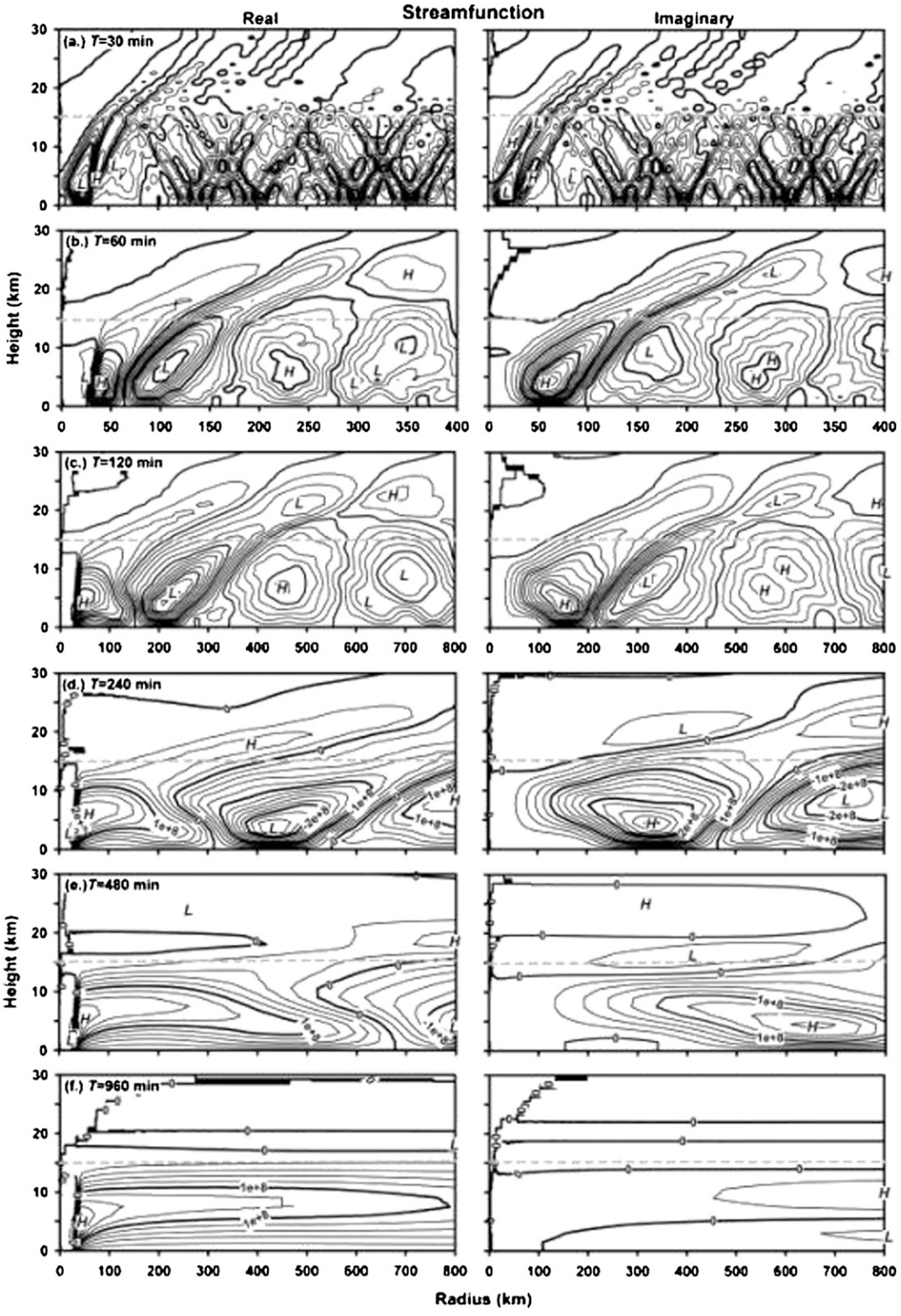

FIG. 4. Real and imaginary parts of the mass flow streamfunction calculated with (10) for eyewall forcing with periods of (a) 30, (b) 60, (c) 120, (d) 240, (e) 480, and (f) 960 min at 20° latitude. For clarity, darker contours, at intervals of 1×10^8 kg s^{-1} throughout, are labeled only in (d)–(f).

entirely of propagating waves. In the imaginary part of ψ with a 60-min period (Fig. 4b), the dipole transforms into an outward-sloping wave crest that extends from $r = 50$ km at the surface to $r = 250$ km at 25-km altitude in the stratosphere after 15 min. After 30 min (minus the real part of ψ), the dipole becomes negative because the heating has switched to cooling. It is surrounded by the negative the original wave pattern now extending from 80 km at the surface to ~300 km in the stratosphere. After 45 min the crest from the initial heating pulse has moved to 50 km at the surface and appears to break up into tropospheric and stratospheric gyres. Indeed the pattern of tropospheric flow for $r > 200$ km is characterized by vertically trapped, outward-propagating waves, with a 200–250-km wavelength that increases as the waves move outward.

When the period is increased to 120 min, the same pattern reappears, but with larger horizontal scale (Fig. 4c). Here, D^4 is positive inside a truncated cone from $r = 50$ km at the surface to the eyewall at 13-km altitude (not shown). Thus, the solutions in the core of the vortex are elliptic, even though they are hyperbolic elsewhere. The same wave pattern reappears. The first two crests exhibit vertical propagation into the stratosphere and a vertically trapped wave train propagates outward in the troposphere. As one might expect from the lower frequency, the waves are about twice as long radially as in Fig. 4b (note horizontal scale change).

Another doubling of the period to 240 min (Fig. 4d) makes the phase and group velocities still more horizontal. Some wave leakage into the stratosphere remains, but the waves are again both twice as long, radial wavelength ~800 km, and trapped below the tropopause to a greater extent. As shown in Fig. 3b, (9) is elliptic within a larger truncated conical volume surrounding the center. There, the solutions are quasi-steady, forced secondary flows that match onto the propagating waves across the locus where D^4 changes sign. A positive streamfunction gyre fills the volume and extends outside of it, from the heat source to $r = 300$ km at the surface. Because it overlaps the hyperbolic subdomain, its outer portion is a propagating extension of the forced circulation. The imaginary part of ψ overlaps this feature and lags behind it by $\pi/2$ both radially and temporally. It is in this region of overlapping waves just outside the boundary between the elliptic and hyperbolic subdomains where the matching of the two solutions takes place.

Increasing the period to 480 min again doubles the horizontal wavelength and further reduces the amount of vertical propagation. The real eyewall streamfunction gyre extends to 600 km, more than twice as far from the center as the elliptic-hyperbolic boundary. The imaginary gyre (which represents this feature after 240 min of propagation) overlaps it inward to $r = 175$ km, approximately the boundary between evanescent and propagating solutions. In the real part of ψ, a negative gyre appears near the boundary of the illustrated subdomain. This feature is the wave crest from the previous forcing cycle. In the stratosphere a pattern low-amplitude waves appears Their phase propagation is upward and outward, equivalent to downward and outward propagation of wave energy.

The longest period, 960 min, forcing produces a ψ field that most closely resembles the SEQ solutions (Fig. 4f). It has deep low-level ($z < 4$–6 km) inflow and deep outflow ($z = 9$–15 km) extending from the eyewall to 800 km. Here the elliptic-hyperbolic boundary is at about $r = 275$ km at the surface and at $r = 18$ km in the upper troposphere. Thus, much of this SEQ-like solution is actually made up of propagating waves. The ψ field has an inner dipole that straddles the heating and supports the eyewall updraft in phase with the forcing. The outer, positive gyre of the dipole is larger and stronger. It sustains the deep inflow and outflow. A second positive gyre straddles the outer boundary of the illustrated subdomain. It supports rising motion in the middle troposphere from about 650 km inward to 150 km, approximately the elliptic-hyperbolic boundary at that level. Above the outermost positive gyre is a positive imaginary gyre, which is in turn overlain by a weak negative imaginary gyre. There may be a faint, negative real gyre between these two features. If so, it is obscured by the strong gradient in the inflow. This pattern of ψ gyres is consistent with a train of long waves between the 200- and 800-km radius. This wave train has upward-propagating phase, implying downward group velocity and wave energy propagation. A possible explanation is reflection or downward scattering of waves originally emitted upward (in terms of energy) across the sloping elliptic-hyperbolic boundary. The scattering is due to the increase in N^2 across tropopause.

In Fig. 4 the half-pendulum day is 35 h at 20° latitude. Repeating the identical calculation at 40° latitude (Fig. 5), where the half pendulum day is 18 h significantly reduces the vertical propagation, but leaves the outer imaginary gyres in place although the outer real gyre is masked. For high-frequency forcing the solutions are nearly the same as Fig. 4. For periods of 240 and 480 min (Figs. 5d,e), the waves have somewhat longer radial lengths, but otherwise differ only in detail from Fig. 4. At higher frequencies (Figs. 5a–c) the ψ fields are again essentially identical with Fig. 4.

If the heat source is moved outward to $r = 60$ km, the amplitude of ψ approximately doubles for all forcing periods because the volume of the heating torus doubles (Fig. 6). With a forcing period of 60 min (Fig. 6b),

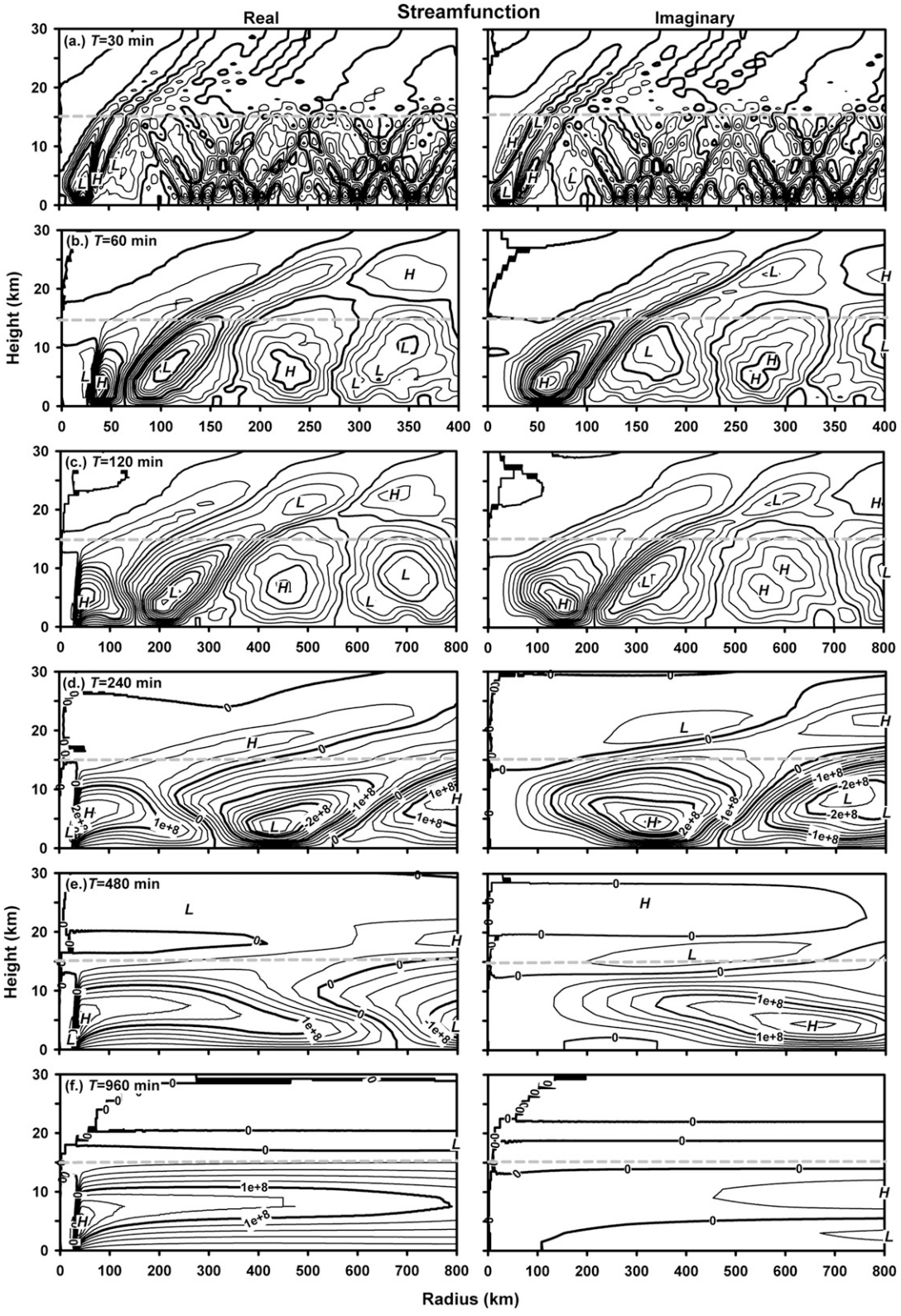

FIG. 5. As in Fig. 4, but at 40° latitude.

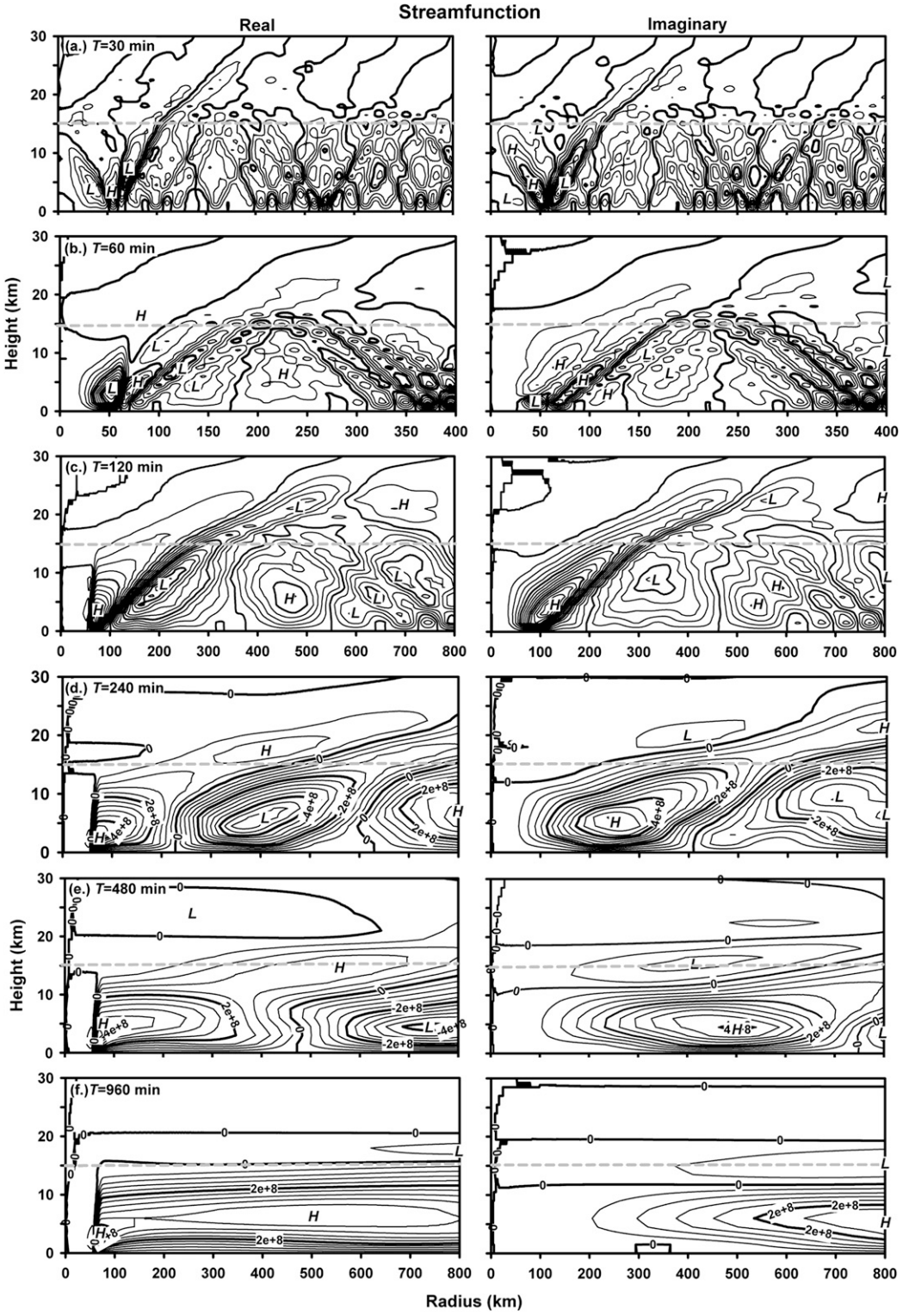

FIG. 6. As in Fig. 4, but with the forcing moved outward to 60 km, twice the eye radius, and the darker contour interval is 2×10^8 kg s^{-1}.

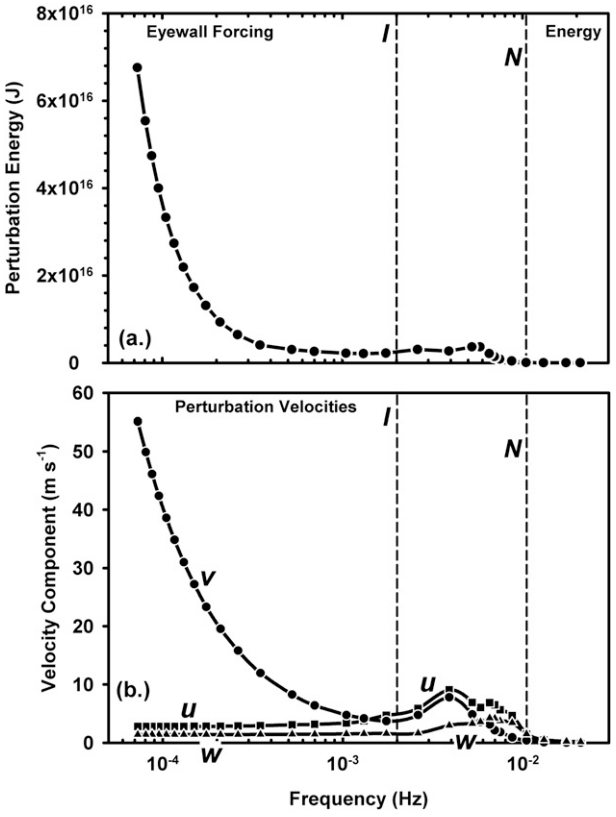

FIG. 7. (a) Wave energy as a function of forcing frequency for eyewall forcing at 20° latitude. (b) Maximum radial, tangential, and vertical velocities as functions of frequency.

there is much more vertical propagation than in Fig. 4b because the forcing is on the hyperbolic side of the elliptic-hyperbolic boundary. Apart from larger amplitude and differences in phase and location due to the different position of the heating, the higher-frequency streamfunction fields are broadly consistent with Figs. 4 and 5.

The total wave energy (Fig. 7a) for the simulations in Fig. 4 is the sum of the wave kinetic and available potential energies times the density integrated over the domain, V:

$$E = \int\int\int_V \frac{1}{2}\rho_0 \left(u^2 + v^2 + w^2 + \frac{b^2}{N^2} \right) dV.$$

It is small when $\omega < N$ because of the impedance mismatch between the forcing and vertical motion. As ω decreases and enters the local inertia buoyancy passband in the neighborhood of the forcing, the wave energy becomes larger, reaching a local maximum about 2/3 of the way across the passband. Here, E has a broad minimum above $\omega = I'$, then it begins to increase, reaching a value of 7×10^{16} J at a frequency of 10^{-4} Hz, well below the Coriolis frequency at 20° latitude.

The domain maximum velocity components (Fig. 7b) explain the variations of wave energy. The radial and vertical velocity components increase from small values just above the passband, reaching maxima near or a bit above the center of the passband. The perturbation buoyancy remains small, again consistent with Eastin et al. (2005a,b) and the analysis in section 3, indicating a robust balance between heating and rising motion against the stable stratification implicit in (4). Although one might naively expect that section 2 and Willoughby (1978, 1979) predict a resonant response to periodic heating at the passband boundaries, no resonances are evident because the flow must obey mass continuity and there is no parallel resonant response in the velocity components perpendicular to those that appear to be singular in (15a) or (15b).

The strong increase in the tangential velocity clearly accounts for the large wave energy at low frequencies. The reason v increases so much lies in the balanced response to heating within the elliptic-hyperbolic boundary. As described by the SEQ, heating in the eyewall forces flow across the RMW into the high angular momentum vortex core, leading to increasing v_o at the RMW and inward from it. This ''convective ring process'' is responsible for the observed contraction of the eyewall as the maximum wind increases in response to convective heating. As the frequency decreases, the duration of the heating and cooling phases of the cycle increase so that the balanced convective ring response has more time to increase v. In addition, lower frequencies move the elliptic-hyperbolic boundary farther away from the heating so that less of the diabatic energy is lost to propagating waves and more goes into the balanced response.

5. Conclusions

The equation for the circumferential component of the vorticty induced by periodic diabatic forcing is closely analogous to the Sawyer–Eliassen equation (SEQ) for the secondary circulation induced on a hurricane-like vortex by steady imposed heating. Both yield solutions expressed as the mass-flow streamfunction, ψ, in the radius–height (r–z) plane. The most significant difference between the equations lies in the coefficients of the second partial derivatives with respect to radius and height. The coefficient of $\partial^2\psi/\partial r^2$ in the circumferential vorticity equation is $N^2 - \omega^2$, where N^2 is square of the buoyancy frequency and ω^2 is the square of the frequency imposed by the forcing instead of simply N^2 as in

the SEQ. Similarly, the coefficient of $\partial^2\psi/\partial z^2$ is in the circumferential vorticity equation is $I'^2 - \omega^2$, where I'^2 is the isobaric local inertia frequency, instead of I'^2 alone. The less highly differentiated terms in these equations are closely analogous, but not identical. Although circumferential vorticity equation describes linear perturbations on a mean vortex in gradient and hydrostatic balance, the perturbations may depart from balance. By contrast, the gradual changes modeled with the SEQ remain balanced as they evolve.

So long as the basic vortex is symmetrically stable, the SEQ is elliptic. By contrast the circumferential vorticity equation is elliptic for frequencies somewhat lower than the local inertia frequency, but hyperbolic for a passband of frequencies approximately bounded by the local inertial and buoyancy frequencies. The mean baroclinity in realistic vortices broadens the passband. Since the inertia frequency approaches the Coriolis frequency on the vortex periphery, the passband becomes wider in frequency space father from the vortex center.

Thus, in the vortex core where the inertia period is measured in terms of fractions of an hour to several hours, periodic heating readily forces temporally varying but balanced responses. Across the boundary where the circumferential vorticity equation becomes hyperbolic, these motions match onto propagating inertial-buoyancy waves. Since the forcing period has to be >2 h for an elliptic subdomain to exist, the group and phase velocities are nearly horizontal and the waves are often trapped in a waveguide formed beneath the increase in static stability at the tropopause. Radiation of inertia-buoyancy waves to the environment can always occur unless the forcing period is longer than a pendulum day.

These results affect understanding of the role of transient convection in hurricane intensification (e.g., Heymsfield et al. 2001). In terms of Fourier series, axially symmetric pulses of convective heat release are represented as a superposition of steady heating and several sinusoidal components. Since the sinusoidal components cause no net heating, only the steady heating changes the vortex intensity permanently, consistent with Nolan and Montgomery (2002) and Nolan and Grasso (2003). Low-frequency sinusoidal components produce Sawyer-Eliassen-like additional intensification during their heating phases and mirror image weakening during their cooling phases. The net effects of both phases approximately cancel. High-frequency components excite inertia buoyancy waves that propagate out of the vortex with little effect on intensity. The reported association of asymmetric convective outbursts with the transitions from weakening to intensification or intensification to weakening may stem from the existence of an optimum amount of shear for asymmetric convection. If so, vortices pass through the optimum on their ways either from shear-limited intensity to intensification or from intensification to shear-induced weakening, in increasing or decreasing shear, respectively.

Radiating inertia-buoyancy waves may be a mechanism by which shear limits tropical cyclone intensity. In a sheared environment, convective cells form on the downshear side of the eyewall, advect with the swirling wind halfway around the eye, and dissipate on the upshear side (Black et al. 2002). Since the cells move with 50%–90% of $V_{\max}$, the wind at the radius of maximum wind $R_{\max}$, the fundamental period of this forcing is thus between the orbital period of the air moving with the wind in the eyewall and about half that value. Much of the resulting heating projects substantially onto asymmetric modes, but both periodic and steady symmetric components will be present as well. The lowest possible frequency for the fundamental is about the local inertial frequency, $\sim\sqrt{2}v_{\max}/r_{\max}$. All of the other components will be propagating. As more of the heating projects onto propagating modes, less will be available to intensify the vortex. Nonetheless, if the steady heating is present, as it must be if there is net convective heat release, it will produce intensification consistent with Nolan and Montgomery (2002) and Nolan and Grasso (2003).

Salient unanswered questions are the magnitude of the energy radiated to the environment and whether or not this mechanism constitutes a significant energy sink for intensifying cyclones. Does it need to be included in energy balance MPI theories (e.g., Bister and Emanuel 1998)? Since waves radiated from tropical cyclones with periods of several hours have nearly horizontal group velocities, they should be detectable with appropriate surface instruments and signal processing.

Acknowledgments. I am grateful to A. G. Pendergrass for insightful comments and discussions. This work was supported by NSF Grant ATM-0454501.

REFERENCES

Bister, M., and K. A. Emanuel, 1998: Dissipative heating and hurricane intensity. *Meteor. Atmos. Phys.,* **65,** 233–240.

Black, M. L., J. F. Gamache, and F. D. Marks Jr., C. E. Samsury, and H. E. Willoughby, 2002: Eastern Pacific Hurricanes Jimena of 1991 and Olivia of 1994: The effects of vertical shear on structure and intensity. *Mon. Wea. Rev.,* **130,** 2291–2312.

Eastin, M. D., W. M. Gray, and P. G. Black, 2005a: Buoyancy of convective vertical motions in the inner core of intense hurricanes. Part I: General statistics. *Mon. Wea. Rev.,* **133,** 188–208.

——, ——, and ——, 2005b: Buoyancy of convective vertical motions in the inner core of intense hurricanes. Part II: Case studies. *Mon. Wea. Rev.,* **133,** 209–227.

Emanuel, K. A., 1999: Thermodynamic control of hurricane intensity. *Nature,* **401,** 665–669.

Hendricks, E. A., M. T. Montgomery, and C. A. Davis, 2004: The role of ''vortical'' hot towers in the formation of Tropical Cyclone Diana (1984). *J. Atmos. Sci.,* **61,** 1209–1232.

Heymsfield, A., J. Halverson, J. Simpson, L. Tian, and T. P. Bui, 2001: ER-2 Doppler radar (EDOP) investigations of the eyewall of Hurricane Bonnie during CAMEX-3. *J. Appl. Meteor.,* **40,** 1310–1330.

Lindzen, R. S., and H. L. Kuo, 1969: A reliable method for the numerical integration of a large class of ordinary and partial differential equations. *Mon. Wea. Rev.,* **97,** 732–734.

Malkus, J., C. Ronne, and M. Chaffee, 1961: Cloud patterns in Hurricane Daisy, 1958. *Tellus,* **13,** 8–30.

Montgomery, M. T., M. E. Nicholls, T. A. Cram, and A. B. Saunders, 2006: A vortical hot tower route to tropical cyclogenesis. *J. Atmos. Sci.,* **63,** 355–386.

Nolan, D. S., and M. T. Montgomery, 2002: Nonhydrostatic, three-dimensional perturbations to balanced, hurricane-like vortices. Part I: Linearized formulation, stability, and evolution. *J. Atmos. Sci.,* **59,** 2989–3020.

——, and L. D. Grasso, 2003: Nonhydrostatic, three-dimensional perturbations to balanced, hurricane-like vortices. Part II: Symmetric response and nonlinear simulations. *J. Atmos. Sci.,* **60,** 2717–2745.

Ooyama, K., 1969: Numerical simulation of the life cycle of tropical cyclones. *J. Atmos. Sci.,* **26,** 3–40.

Pearce, R. P., 2004: An axisymmetric model of a mature tropical cyclone incorporating azimuthal vorticity. *Quart. J. Roy. Meteor. Soc.,* **130,** 259–293.

——, 2005: Why must hurricanes have eyes? *Weather,* **60,** 19–24.

Pendergrass, A. G., and H. E. Willoughby, 2009: Diabatically induced secondary flows in tropical cyclones. Part I: Quasi-steady forcing. *Mon. Wea. Rev.,* **137,** 805–821.

Schubert, W. H., and J. J. Hack, 1982: Inertial stability and tropical cyclone development. *J. Atmos. Sci.,* **39,** 1687–1697.

Shapiro, L. J., and H. E. Willoughby, 1982: The response of balanced hurricanes to local sources of heat and momentum. *J. Atmos. Sci.,* **39,** 378–394.

Simpson, J., J. B. Halverson, B. S. Ferrier, W. A. Petersen, R. H. Simpson, R. Blakeslee, and S. L. Durden, 1998: On the role of ''hot towers'' in tropical cyclone formation. *Meteor. Atmos. Phys.,* **67,** 15–35.

Smith, R. K., 1981: The cyclostrophic adjustment of vortices with application to tropical cyclone modification. *J. Atmos. Sci.,* **38,** 2021–2030.

——, 2005: Why must hurricanes have eyes? Revisited. *Weather,* **60,** 326–328.

——, M. T. Montgomery, and H. Zhu, 2005: Buoyancy in tropical cyclones and other rapidly rotating vortices. *Dyn. Atmos. Oceans,* **40,** 189–208.

Sundquist, H., 1970: Numerical simulation of the development of tropical cyclones with a ten-level model. Part I. *Tellus,* **22,** 369–390.

Willoughby, H. E., 1978: The vertical structure of hurricane rainbands and their interaction with the mean vortex. *J. Atmos. Sci.,* **35,** 849–858.

——, 1979: Excitation of spiral bands in hurricanes by interaction between the symmetric mean vortex and shearing environmental current. *J. Atmos. Sci.,* **36,** 1226–1235.

——, J. A. Clos, and M. B. Shoreibah, 1982: Concentric eyewalls, secondary wind maxima, and the development of the hurricane vortex. *J. Atmos. Sci.,* **39,** 395–411.

——, R. W. R. Darling, and M. E. Rahn, 2006: Parametric representation of the primary hurricane vortex. Part II: A new family of sectionally continuous profiles. *Mon. Wea. Rev.,* **134,** 1102–1120.